Structures 51 (2023) 602–614

Contents lists available at ScienceDirect

Structures

journal homepage: www.elsevier.com/locate/structures

Derivation of shear enhancement factor β used in FprEN1992 to calculate design shear force at corner columns of flat slabs

Deema Abu-Salma [a], Robert L. Vollum [b,*], Lorenzo Macorini [c]

[a] Department of Civil and Environmental Engineering, Imperial College London, London, United Kingdom
[b] Professor of Structural Concrete, Department of Civil and Environmental Engineering, Imperial College London, London, United Kingdom
[c] Reader in Structural Engineering, Department of Civil and Environmental Engineering, Imperial College London, London, United Kingdom

ARTICLE INFO

Keywords:
Punching shear
Flat slabs
Critical Shear Crack Theory
Corner column connections
Shear field analysis

ABSTRACT

The next generation of Eurocode 2 (FprEN 1992) adopts a closed form version of the Critical Shear Crack Theory (CSCT) for punching shear design. The code accounts for loading eccentricity by multiplying the design shear force by a coefficient β. The paper describes the derivation of the expression adopted in FprEN 1992 for β at corner columns of flat slabs. The proposed formula is validated for normal size columns, with maximum side length less than 3d, where d is the slab mean effective depth, and non-square columns with long side greater than 3d. Due to the absence of experimental data on punching resistance at non-square corner columns, the derived formula is validated for such columns using NLFEA with 3-D solid elements. Comparisons are also made with punching resistances determined using the classic CSCT in which punching resistance is explicitly related to slab rotation relative to the support. The closed form CSCT is shown to predict punching shear resistance well, when used in conjunction with the proposed β factor.

1. Introduction

The next generation of Eurocode 2 [1] is due to be released in 2023. The technical content of the revised code [1] has now been finalised following public enquiry. An area of the code with significant changes is design for punching shear. The revised design rules (FprEN1992 [1]) are based on the Critical Shear Crack Theory [2], which relates punching resistance to slab rotation. In its original "classic" form punching resistance is found from the intersection of the load-rotation and load-resistance curves. This presentation, which is implemented in fib Model Code 2010 [3], was deemed too radical for inclusion in the revised code. Consequently Muttoni et al. [4] developed a closed form solution for the equations of the CSCT which is implemented in FprEN1992 [1]. In this approach, the influence of loading eccentricity is accounted for by increasing the design shear force by a multiple β as done in EC2 (2004) [5]. The paper describes the derivation and validation of the expression adopted for βat corner columns in FprEN1992. The expression is derived using shear field analysis [6,7] of representative full scale flat slab to corner column connections and then validated using test data from the literature and NLFEA of corner column punching specimens with non-square columns which have not been tested experimentally. The NLFEA is carried out using ATENA [8] with 3-D solid elements and for comparison the classic CSCT in which rotations are calculated using NLFEA. The CSCT failure load is determined both through post processing as in fib Model Code 2010 Level of Approximation IV (LoA IV) [3] and in a Joint Shell Punching Model (JSPM) [9].

Pertinent experimental studies, which are relatively few, are those of Hammill and Ghali [10], Ingvarsson [11], Stamenkovic and Chapman [12], Sudarsana [13], Vocke [14], Walker and Regan [15], Zaghlool [16] and Zaghlool et al. [17]. All the tested specimens had square columns. The specimens of [10–12,15,16] were isolated statically determinate specimens with fixed loading eccentricities of typically equal magnitude along each slab edge. Those of [17] were single panel table-top specimens with columns provided just below the slab. Walker and Regan [15] tested both single panel table-top specimens and single panel slabs with relatively large corner columns extending above and below the slab. Sudarsana [13] individually tested to failure the corner column connections of a four bay continuous flat slab. Details of all these specimens are summarised in Table 1 in which isolated and continuous slabs are denoted I and C respectively.

* Corresponding author.
E-mail address: r.vollum@imperial.ac.uk (R.L. Vollum).

https://doi.org/10.1016/j.istruc.2023.03.049
Received 17 December 2022; Received in revised form 7 March 2023; Accepted 8 March 2023
Available online 21 March 2023

1.1. Critical shear crack theory

In the classic CSCT [2], punching failure occurs at the intersection of the load-rotation and resistance-rotation curves. MC2010 provides four levels of approximation (LoAs) for calculating punching shear resistance. In LoA IV, which is the most accurate, rotations are determined with nonlinear finite element analysis (NLFEA). Fig. 1 shows the basic control perimeter $b_{0,5}$ adopted in the CSCT for punching at corner columns. As shown, the control perimeter is positioned at half the slab shear effective depth (d_v) from the column face. For the specimens investigated in this paper, d_v equals the slab effective depth (d). The maximum length of the straight sides of the perimeter is limited to $3d_v$ as shown in Fig. 1b.

To account for the effect of loading eccentricity, the length of the shear resisting control perimeter is calculated in the classic CSCT using equation (1) in which $b_{0,5}$ is defined in Fig. 1:

$$b_{0,MC2010} = k_e b_{0,5} \tag{1}$$

In floors where the difference in adjacent spans is no more than 25 % in length, k_e may be taken as 0.9, 0.7 and 0.65 for interior, edge and corner columns respectively. Otherwise, k_e may be calculated using equation (2) below:

$$k_e = \frac{1}{(1 + \frac{e_u}{b_u})} \tag{2}$$

in which:

$$e_u = \sqrt{e_x^2 + e_y^2} \tag{3}$$

e_x and e_y are the eccentricities of the line of action of the support forces with respect to the centroid of the control perimeter and b_u is the diameter of a circle with the same enclosed area as the control perimeter. The full control perimeter is used for the calculation of terms in k_e without the reduction in length for column sides longer than $3d_v$ shown in Fig. 1b. For calculation of e_x and e_y, the control perimeter is approximated with square corners.

MC2010 also permits shear field analysis to be used to determine the shear resisting perimeter as follows:

$$b_{0,MC2010} = \frac{V_{Ed}}{v_{perp,d,max}} \tag{4}$$

where $v_{perp,d,max}$ is the maximum shear force per unit length perpendicular to the control perimeter. $v_{perp,d,max}$ can be found from elastic finite element analysis.

This paper adopts the mean strength failure criterion of Muttoni [2] in the calculation of punching resistance using the CSCT.

1.2. Closed form formulation of CSCT

In FprEN1992, the equations of the closed form CSCT (Muttoni et al. [4]) are expressed as follows.

$$\tau_{Ed} = \beta \frac{V_{Ed}}{b_{0,5} d_v} \tag{5}$$

in which τ_{Ed} is the design shear stress, β, which is the main concern of this paper, accounts for eccentric shear, V_{Ed} is the design shear force, $b_{0,5}$ is the punching control perimeter (see Fig. 1) and d_v is the shear resisting effective depth.

Table 1
Database of tests with corner slab-column connections.

Author	Slab reference/ type		c mm	h mm	d mm	f_c' MPa	f_y MPa	ρ %	V_{test} kN	M_{test} in x kNm	M_{test} in y kNm
Zaghlool [16]	Z-I (1)	I	178.0	152.4	120.6	32.7	379.2	1.23	74.3	19.2	19.2
	Z-II (1)	I	266.7	152.4	120.6	33.0	388.9	1.23	137.9	38.5	38.5
	Z-II (2)	I	266.7	152.4	120.6	33.4	405.4	1.65	177.2	53.4	53.4
	Z-II (3)	I	266.7	152.4	120.6	27.7	450.9	2.23	177.9	58.0	58.0
	Z-II (5)	I	266.7	152.4	120.6	34.8	381.3	1.23	148.6	0.00	0.00
	Z-II (5d)	I	266.7	152.4	120.6	34.3	381.3	1.23	138.0	0.00	0.00
	Z-II (6)	I	266.7	152.4	120.6	33.6	381.3	1.23	82.3	38.9	38.9
	Z-III (1)	I	355.6	152.4	120.6	33.6	379.2	1.23	179.7	52.7	52.7
Stamenkovic and Chapman [12]	C/C/1	I	127.0	76.2	55.6	30.4	448.0	1.17	24.9	6.24	0.00
	C/C/2	I	127.0	76.2	55.6	28.3	448.0	1.17	15.9	6.38	0.00
Hammill and Ghali [10]	NH1	I	250.0	150.0	114.0	41.5	440.0	1.76	146.9	43.0	43.0
	NH2	I	250.0	150.0	114.0	42.2	440.0	1.76	139.1	40.2	40.2
Zaghlool et al. [17]	I	C	139.7	139.7	114.3	24.1	379.2	1.47	107.6	10.4	8.76
	III	C	165.0	139.7	114.3	20.7	379.2	1.47	101.5	16.0	16.0
	IV	C	165.0	139.7	114.3	35.8	379.2	1.47	122.5	15.7	22.0
Walker and Regan [15]	SC1	C	300.0	125.0	100.0	43.3	450.0	0.65	81.5	25.2	25.2
	SC2	C	300.0	125.0	100.0	47.9	450.0	0.41	74.8	24.0	24.0
	SC3	C	300.0	125.0	100.0	37.4	450.0	0.83	74.2	31.6	31.6
	SC4	C	220.0	125.0	100.0	40.8	450.0	0.65	63.8	16.7	16.7
	SC5	C	220.0	125.0	100.0	46.5	450.0	0.93	82.2	18.8	18.8
	SC7	C	220.0	125.0	100.0	43.8	450.0	0.93	82.2	27.6	27.6
	SC8	C	160.0	80.0	64.0	37.4	595.0	0.28	33.0	4.70	4.70
	SC9	C	160.0	80.0	64.0	34.3	595.0	0.56	33.0	5.90	5.90
	SC11	C	160.0	80.0	62.0	27.2	595.0	0.96	33.0	4.60	2.20
	SC12	C	300.0	80.0	62.0	40.7	595.0	0.79	36.8	12.7	8.90
Ingvarsson [11]	I1	I	180.0	120.0	95.0	25.8	454.0	2.17	108.0	21.2	21.2
	I2	I	180.0	120.0	95.0	33.3	454.0	1.10	76.0	16.3	16.3
	I4	I	180.0	120.0	95.0	32.0	454.0	1.10	101.0	17.7	17.7
	I5	I	180.0	120.0	95.0	29.2	454.0	1.77	110.0	22.6	22.6
Sudarsana [13]	C6	C	305.0	140.0	105.0	44.4	420.0	0.98	108.6	34.9	34.9
	C7	C	305.0	140.0	105.0	44.4	420.0	0.98	93.7	33.0	33.0
	C8	C	305.0	140.0	105.0	44.4	420.0	0.98	98.1	27.5	27.5
Vocke [14]	E1	I	300.0	230.0	189.0	23.6	540.0	1.07	305.0	61.4	61.4
	E3	I	300.0	230.0	189.0	31.8	540.0	1.28	351.0	65.1	65.1

Note: c = column side dimension, h = slab depth, d = effective depth, f_c' = concrete cylinder strength, ρ = flexural reinforcement ratio, M_{test} = moment about column centreline.

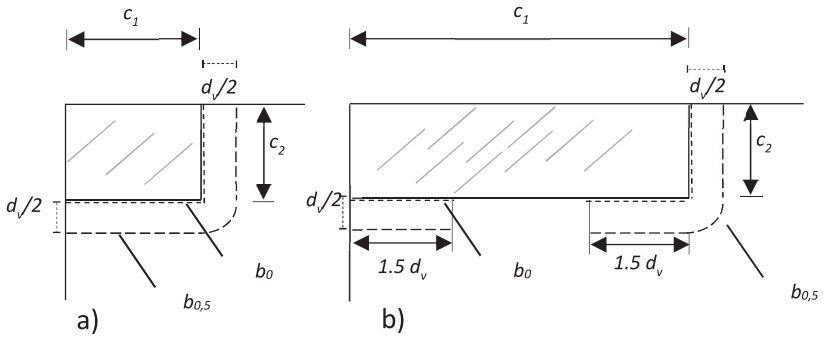

Fig. 1. MC2010 and FprEN1992 basic control perimeter $b_{0,5}$ for a) c_1 and $c_2 < 3d_v$ (b_1) and b) $c_1 > 3d_v$ and $c_2 < 3d_v$.

FprEN1992 allows β to be taken as 1.5 at corner columns if the slab is uniformly loaded and:

- The lateral stability does not depend on frame action;
- Adjacent spans don't differ by more than 25 %;
- The moment transferred to the column about the x and/or y axes (see Fig. 2) does not exceed $M_{t,max} = 0.25 b_e d^2 f_{cd}$ where b_e is defined for both column sides in contact with the slab as shown in Fig. 2 and f_{cd} is the design concrete compressive strength.

The limiting column transfer moment $M_{t,max}$ is taken from Annex I of EC2 (2004) [5], which is informative.

FprEN1992 also gives refined expressions for punching shear at internal, edge and corner columns. The development of the refined expression for β at corner columns is the subject of this paper.

The design shear stress τ_{Ed} should not exceed the design shear resistance which is given by:

$$\tau_{Rd,c} = \frac{0.6}{\gamma_v} k_{pb} \left(100 \rho f_{ck} \frac{d_{dg}}{d_v}\right)^{1/3} \leq \frac{0.5}{\gamma_v} \sqrt{f_{ck}} \tag{6}$$

where k_{pb}, in which b_0 is defined in Fig. 1, is determined as follows:

$$1 \leq k_{pb} \leq 3.6 \sqrt{1 - \frac{b_0}{b_{0,5}}} \leq 2.5 \tag{7}$$

and $\rho = \sqrt{\rho_x \rho_y}$ is the flexural tension reinforcement ratio in which $\rho_x = A_{sx}/b_{sx}d_x$, $\rho_y = A_{sy}/b_{sy}d_y$ in which b_{sx} and b_{sy} are defined at corner columns as shown in Fig. 3. The coefficient γ_v is the partial factor for shear which is 1.4 for design and 1.0 in the strength assessments of this paper. The coefficient d_{dg} is the reference value for the critical shear crack roughness calculated as:

$$d_{dg} = d_{g0} + d_g . min\left(\left(\frac{60}{f_{ck}}\right)^2, 1\right) \leq 40mm \tag{8}$$

in which f_{ck} is the characteristic concrete uniaxial compressive strength, $d_{g0} = 16$ mm for normal concrete and d_g is the maximum aggregate size. For distances a_p smaller than 8 d_v, the value of d_v used in equation (6) may be replaced by:

$$a_{pd} = \sqrt{\frac{a_p}{8} d_v} \tag{9}$$

where $a_p = \sqrt{a_{px} a_{py}} \geq d_v$ in which a_{px} and a_{py} are measured from the centroid of the control perimeter to the positions where the bending moments $m_{Ed,x}$ and $m_{Ed,y}$ are zero along the x-and y-axis respectively. According to FprEN1992, for corner columns of flat slabs where the lateral stability does not depend on frame action between the slabs and the columns, a_p may be approximated as $a_p = 0.22L$ where L is the largest span length of the adjacent bays in either the x- or y direction.

1.2.1. Derivation of β in FprEN1992

The authors derived the expression for β at corner columns in FprEN1992 using a similar procedure to that they adopted for punching at edge columns [18]. For consistency with the format adopted for k_e in MC010 (see equation (2), β was initially defined as:

$$\beta = \frac{1}{k_e} = 1 + \frac{e_u}{b_u} \tag{10}$$

Equation (10) for β was subsequently simplified, for ease of use, in FprEN 1992 as follows:

$$\beta = 1 + 1.1 \frac{e_b}{b_b} \geq 1.05 \tag{11}$$

in which b_b is the geometric mean of the maximum and minimum overall side lengths of the control perimeter at $0.5d_v$ approximated with square corners. The full side lengths of the control perimeter are used in the calculation of b_b without reduction in length for column sides greater in length than $3d_v$. For consistency with their [18] treatment of biaxially loaded edge columns as presented in FprEN1992, the authors defined e_b

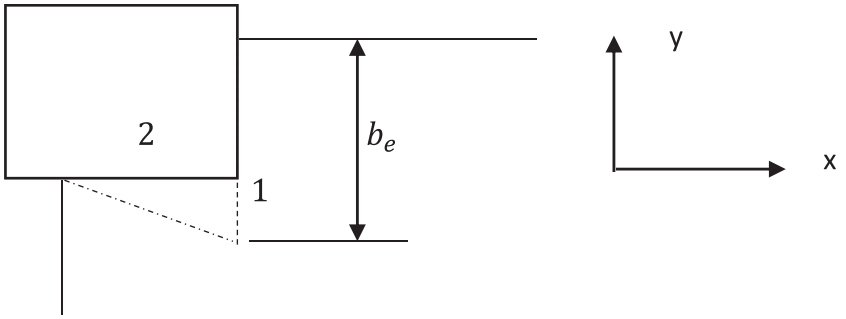

Fig. 2. Definition of b_e.

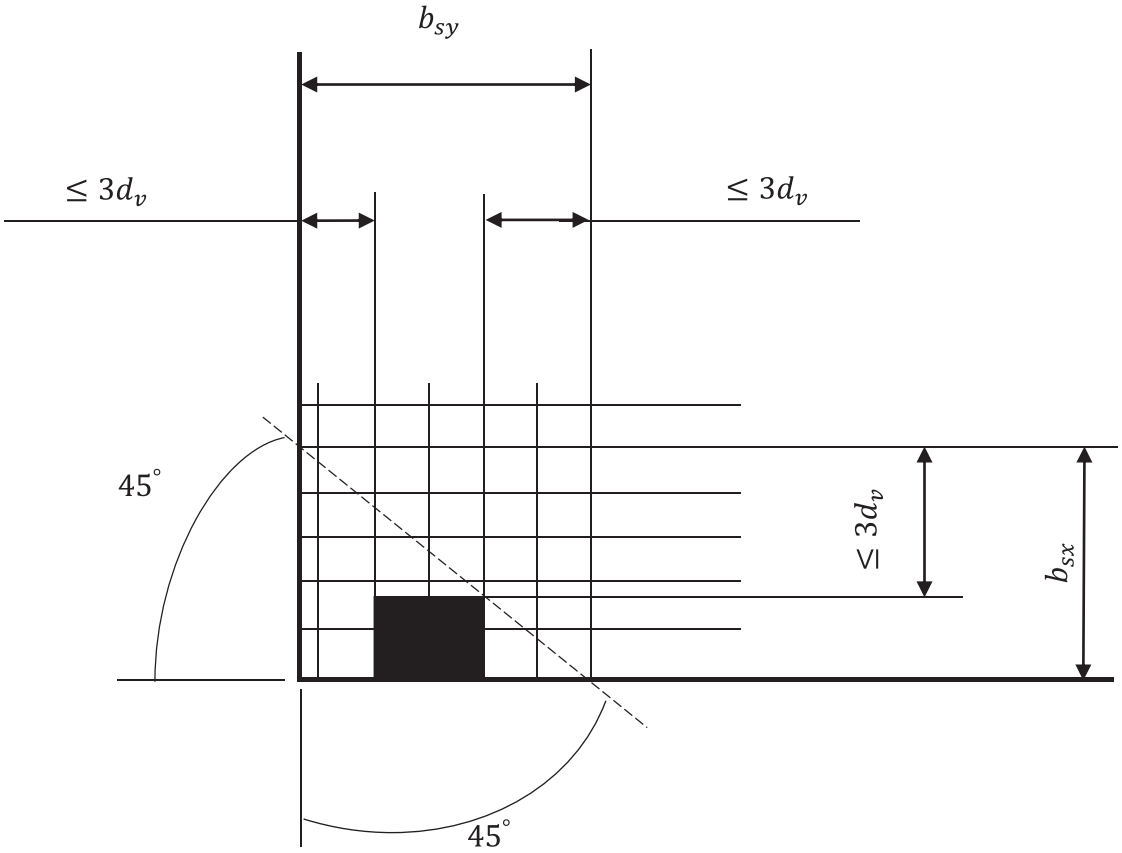

Fig. 3. Definition of b_s.

for corner columns as $e_b = k(|e_x| + |e_y|)$ where e_x and e_y are defined below equation (3). Calibration of Equation (11) involves determining k.

The proposed expression for β was derived using shear field analysis, as allowed by FprEN1992, and then validated using test data and NLFEA of virtual specimens with geometries not represented in the experimental database. Clause 8.4.2(7) of FprEN1992 allows the design shear force around the punching control perimeter to be obtained with elastic finite element analysis. Furthermore, the clause allows the shear force to be averaged over a maximum distance of $2d_v$ to either side of the peak provided equilibrium is maintained. This approach is consistent with that of Setiawan et al. [6,7] who showed that for elongated internal columns the critical design shear stress to be used in the CSCT can be taken as the average elastic stress around the most highly stressed quadrant of the control perimeter. The approach of [6,7] was found by Abu-Salma et al. [18] to give good predictions of β at edge columns so is also adopted in this paper for the derivation of β at corner columns.

Initially, a parametric study was carried out of a full-scale floor plate of a flat slab building in ETABS [19]. The layout of the building was similar to that used in [18] for derivation of β at edge columns. The column cross section and slab span lengths were varied in the study. Thick shell elements were used to model the slab which was connected to the columns via rigid links. For each bay size, the slab thickness was derived from charts provided in Economic Concrete Frame Elements to Eurocode 2 [20]. The floor-to-floor height was taken as 3 m. The investigated column sizes were 300 x 300, 300 x 600, 300 x 750 and 300 x 1000 mm^2. Bay sizes in metres of 4 x 4, 6 x 6, 8 x 4, 8 x 6, 8 x 8 and 9x 4 were considered. The slab thickness varied between 200 mm and 300 mm. A cladding load of 10 kN/m was applied to the slab edge. The design characteristic superimposed dead and live loads were taken as 1.5 kN/m^2 and 3.0 kN/m^2 respectively. The ratio of column side length to average slab effective depth ranged between 1.1 and 6.1.

Design shear force enhancement factors β_{SF} were calculated for the specimens considered in the parametric study as the ratio of the average shear force around the control perimeter $b_{0,red}$ shown in Fig. 4 to that around the basic control perimeter $b_{0.5}$ shown in Fig. 1. The resulting β_{SF} values are plotted against $1.1(|e_x| + |e_y|)/b_b$ in Fig. 5a which shows that the slope of the line of best fit with intercept equal to 1 is k = 0.27. Consequently, e_b in equation (11) is given by:

$$e_b = 0.27(|e_x| + |e_y|) \tag{12}$$

where e_x and e_y are the eccentricities of the line of action of the support forces with respect to the centroid of the control perimeter. For this purpose, the control perimeter was simplified by replacing parts of circles by corners and not limiting the straight segments to $3d_v$ as done for calculation of resistance. In this paper, β calculated with equations (11) and (12) is referred to as β refined.

Fig. 5b shows that $\beta_{SF}/\beta_{refined}$ is sensibly independent of the loading angle (atan(e_x/e_y)) for the data considered in Fig. 5a. This is significant since the loading angle is 45° for the majority of specimens in the

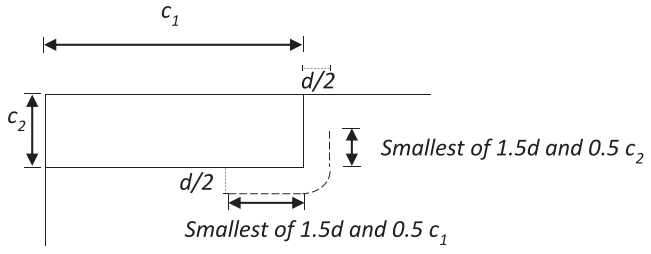

Fig. 4. Segment of control perimeter ($b_{0,red}$) around which shear stress is averaged in shear field analysis for corner columns.

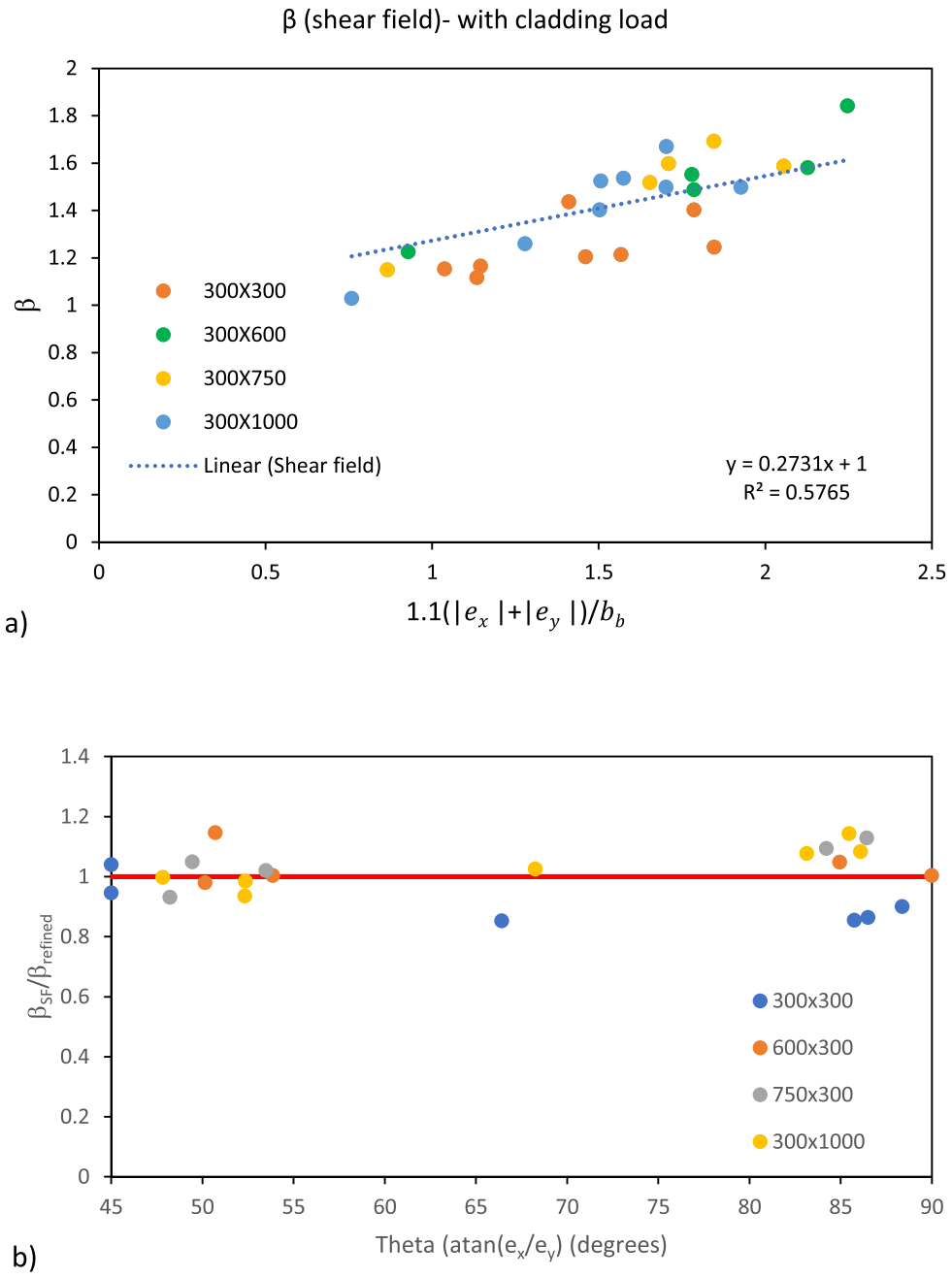

Fig. 5. Influence of a) $1.1(|e_x|+|e_y|)/b_b$ and b) loading angle on $\beta_{SF}/\beta_{refined}$ for corner columns.

experimental database. The loading angle departs from 45° for many of the slabs in Fig. 5 due to the adoption of non-square bays and non-square column cross sections.

In order to comply with FprEN1992, the influence on moment equilibrium of averaging the through thickness shear force (in kN/m) acting on $b_{0,red}$ (see Fig. 4) was investigated. This was done by finding the resultant moment about the centroid of the control perimeter of the shear force acting on $b_{0,red}$ for i) the elastic shear force and ii) the average shear force. The percentage error on moment equilibrium of averaging the shear force around $b_{0,red}$ was found to be minimal, thereby justifying the averaging of shear force in the shear field analysis. Analysis shows β_{sf} to be sensitive to the modelling assumptions and shear stiffness of the adopted shell element. Consequently, it is not recommended that shear field analysis is used for routine design.

The next step in the derivation of β was to validate Equation (12) for the experimental data in Table 1. If the closed form formulation of the CSCT were exact, the coefficient β would be given by V_{calc}/V_{test} where V_{calc} is the strength calculated using the closed form CSCT neglecting eccentricity (i.e. with $\beta = 1$) and V_{test} is the measured strength. In this assessment, f_{ck} was taken as the measured concrete strength from Table 1 and $\gamma_c = 1.0$. Consequently, k can be estimated by plotting V_{calc}/V_{test} against $\frac{1.1(|e_x|+|e_y|)}{b_b}$. This is done in Fig. 6 which shows that taking $k = 0.27$ as in Equation (12) from FprEN1992 provides a reasonable fit to the test data.

Table 2 and Fig. 7 compare the measured punching resistances of the slabs in Table 1 with the predictions of FprEN1992 with d_v in equation (6) replaced by a_{pd} unless noted otherwise. Fig. 7a to 7c evaluate the refined β (see equations (11) and (12)). Fig. 7a shows V_{test}/V_{calc} calculated using the experimental eccentricities at punching failure, while Fig. 7b shows the effect of not replacing d_v with a_{pd} in equation (6). Comparison of the two figures shows that not replacing d_v with a_{pd} in

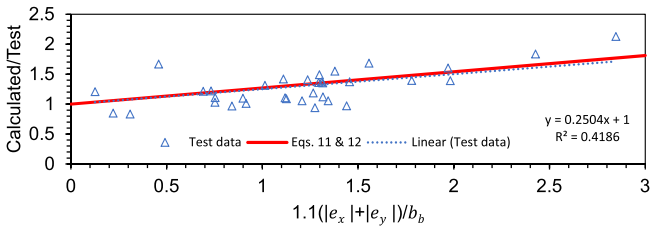

Fig. 6. Derivation of β using regression analysis conducted on experimental slabs.

Table 2
V_{test}/V_{calc} for corner slab-column connections.

Author	Slab reference/type		FprEN1992				EC2 2004 with $M_{n,max}$
			$\beta = 1.5$ with $M_{n,max}$	β refined $(M/V)_{test}$	$(M/V)_{elastic}$	β = 1/ke MC2010 $(M/V)_{test}$	
Zaghlool [16]	Z-I (1)	I	0.89	0.84	0.84	1.13	0.90
	Z-II (1)	I	1.38	1.20	1.20	1.51	1.43
	Z-II (2)	I	1.60	1.43	1.43	1.84	1.66
	Z-II (3)	I	1.55	1.43	1.43	1.88	1.60
	Z-II (5)	I	1.46	1.17	1.17	1.39	1.52
	Z-II (5d)	I	1.36	1.09	1.09	1.29	1.41
	Z-II (6)	I	0.82	0.90	0.90	1.30	0.85
	Z-III (1)	I	1.55	1.27	1.27	1.53	1.63
Stamenkovic & Chapman [12]	C/C/1	I	1.39	1.06	1.06	1.56	1.25
	C/C/2	I	1.53	0.83	0.83	1.42	0.82
Hammill and Ghali [10]	NH1	I	1.42	1.29	1.29	1.68	1.41
	NH2	I	1.34	1.21	1.21	1.57	1.32
Zaghlool et al. [17]	I	C	1.24	0.86	0.89	0.90	1.59
	III	C	1.23	0.98	1.00	1.16	1.51
	IV	C	1.24	0.98	1.01	1.17	1.52
Walker and Regan [15]	SC1	C	1.07	0.95	1.03	1.21	1.21
	SC2	C	1.10	0.99	1.06	1.28	1.25
	SC3	C	0.94	0.96	0.90	1.33	1.07
	SC4	C	0.97	0.89	1.00	1.15	1.12
	SC5	C	1.06	0.92	1.09	1.15	1.22
	SC7	C	1.08	1.10	1.11	1.53	1.24
	SC8	C	1.36	1.13	1.36	1.38	1.82
	SC9	C	1.11	1.00	1.10	1.29	1.48
	SC11	C	0.90	0.67	0.74	0.81	1.40
	SC12	C	1.01	0.91	0.84	1.18	1.36
Ingvarsson [11]	I1	I	1.36	1.18	1.18	1.49	1.73
	I2	I	1.10	0.99	0.99	1.28	1.40
	I4	I	1.49	1.23	1.23	1.51	1.88
	I5	I	1.42	1.26	1.26	1.60	1.80
Sudarsana [13]	C6	C	1.27	1.13	1.13	1.45	1.29
	C7	C	1.09	1.01	1.01	1.33	1.11
	C8	C	1.14	0.97	0.97	1.20	1.16
Vocke [14]	E1	I	1.80	1.30	1.30	1.41	1.71
	E3	I	1.77	1.25	1.25	1.33	1.68
	Mean		**1.27**	**1.07**	**1.09**	**1.36**	**1.39**
	Standard deviation		**0.25**	**0.18**	**0.18**	**0.23**	**0.27**

equation (6) provides additional safety for continuous slabs with low loading eccentricities where a_{pd} can be significantly less than d_v. Consequently, due to the relative lack of experimental data on punching at corner columns, the authors recommend conservatively taking $a_{pd} = d_v$ in equation (6) if using the refined β. In design, the loading eccentricity e_b is calculated using elastic analysis. Therefore, Fig. 7c shows V_{test}/V_{calc} calculated using elastic eccentricities for the continuous slabs and measured eccentricities for isolated slabs. To obtain the elastic eccentricities, a linear elastic analysis was conducted with ETABS [19] assuming the column ends were pinned. Fig. 7d shows that punching resistances are significantly underestimated if β is calculated with equation (10) in accordance with MC2010 taking $e_u = \sqrt{e_x^2 + e_y^2}$ using measured eccentricities e_x and e_y. Finally, Fig. 7e and 7f evaluate $V_{test}/V_{calculated}$ using $\beta = 1.5$ without and with the limit on the maximum moment transfer to the column. The figures suggest that it is prudent to limit the column transfer moment to M_{tmax} when using $\beta = 1.5$ to avoid having unsafe results at high eccentricities.

$V_{test}/V_{calculated}$ was also calculated with EC2 (2004) for the specimens in Table 1 using the reduced basic control perimeter u_{1*} defined in the code. Additionally, the column transfer moment was limited to $M_{t,max} = 0.25 b_e d^2 f_{cd}$ with b_e defined as in Fig. 2. This approach is equivalent to defining a limiting value of β based on a maximum

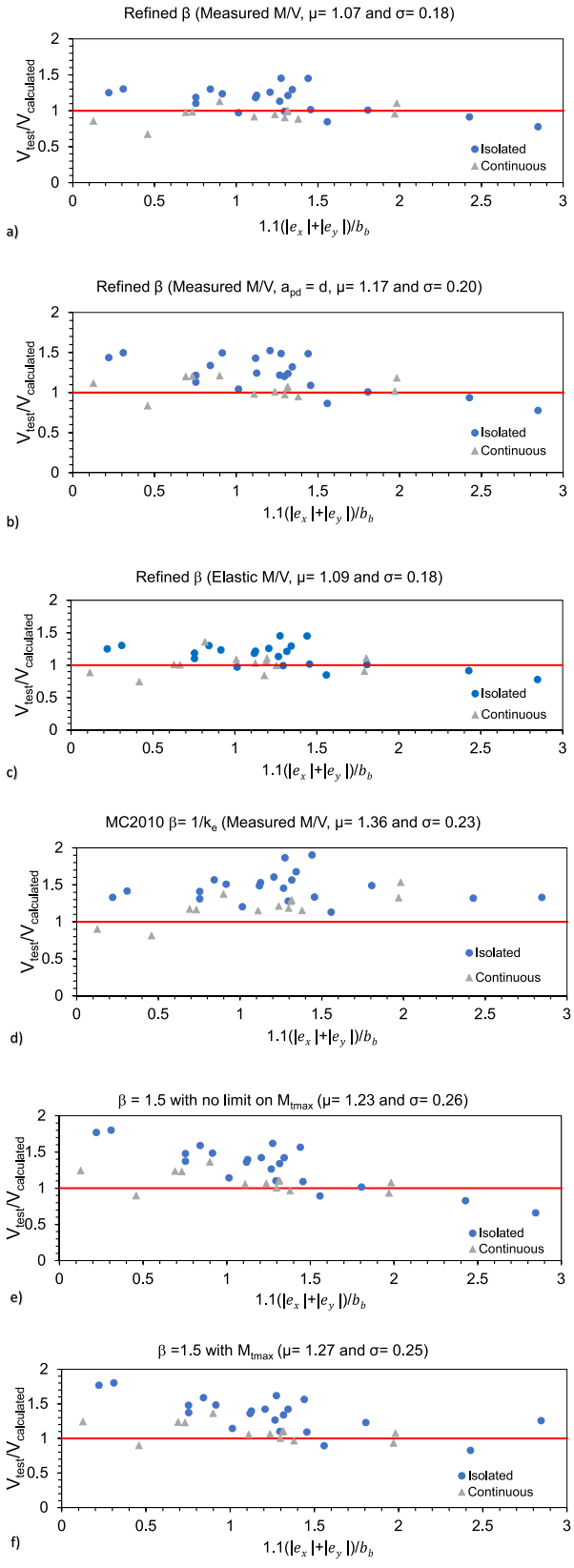

Fig. 7. Evaluation of a) refined β using measured ultimate eccentricities from the test, b) refined β using measured ultimate eccentricities from the test and a_{pd} = d, c) refined β using elastic eccentricities, d) MC2010 expression for e_u using measured ultimate eccentricities from the test, e) $\beta = 1.5$ without limit on M_{tmax} and f) $\beta = 1.5$ with limit on M_{tmax}.

allowable eccentricity corresponding to $M_{t,max}$. The results are presented in Table 2 which shows EC2 (2004) to be relatively conservative compared with FprEN1992.

2. NLFEA of punching failure at corner columns

Owing to the relative scarcity of experimental data on punching at corner columns, this paper uses NLFEA with 3-D solid elements to extend the available database to specimens with columns of varying cross section aspect ratio. The results of the NLFEA with 3-D solid elements are compared with the predictions of the classic CSCT, the authors' JSPME [24] and the closed form formulation of the CSCT in FprEN1992. The NLFEA was initially validated using selected test data from Table 1. Subsequently, the validated NLFEA was used to analyse virtual corner column punching specimens with non-square columns. The resulting punching resistances are shown to compare favourably with the strength predictions of FprEN1992 thereby further justifying the refined β given by equations (11) and (12).

2.1. NLFEA with 3-D solid elements

ATENA [8] was employed to carry out the NLFEA using 3-D solid elements. The adopted modelling procedure was the same as previously adopted by Setiawan et al. [9], who modelled 16 interior slab-column connections, and Abu-Salma et al. [24] who modelled 4 interior column punching tests and 12 edge column punching tests. The mean and standard deviation of $V_{test}/V_{predicted}$ are $\mu = 0.96$ and $\sigma = 0.075$ in [9] and $\mu = 1.02$ and $\sigma = 0.08$ in [24].

The fracture-plastic model CC3DNonLinCementitious2 was used for modelling concrete. In this model, the Rankine [8] tensile failure criterion was utilised with exponential softening. Plasticity for concrete in compression is controlled by the Menetrey-Willam [21] failure surface. The hardening part of the compressive response is related to strain, while the softening part is related to displacement for reasons of mesh objectivity. The compressive softening response is based on Van Mier

Table 3
Modelling parameters adopted in ATENA [6,24].

No.	Parameter	Value/Reference
	Concrete constitutive model	
A1	Concrete elastic modulus	Model Code 2010 [3]
A2	Fracture energy	Model Code 2010 [3]
A3	Concrete tensile strength	Model Code 2010 [3]
A4	Smeared crack model	Fully-rotating crack
A5	Critical compressive displacement w_d	0.5 mm
A6	Limit of compressive strength reduction due to cracking $r_c^{lim} f_c'$	0.8 f_c'
A7	Eccentricity (defining the shape of the failure surface)	0.52
A8	Volume dilatation plastic factor	0
	Reinforcement bar model	
B1	Stress–strain relationship	Bilinear with strain hardening modulus of 0.2 MPa
B2	Bond-slip model	Perfect bond
	Loading procedure and convergence criteria	
C1	Loading procedure	Static (force-controlled)
C2	Solution procedure	Arc-length method
C3	Convergence criteria for displacement, residual force, and absolute residual force error	1 %
C4	Convergence criterion for energy error	0.01 %
	Mesh properties	
D1	Mesh size (finest)	m × m × m mm (10 elements along height)
D2	Mesh element for concrete slab	8-noded hexahedral (linear)
D3	Mesh element for loading apparatus	4-noded tetrahedral (linear)
D4	Mesh element for reinforcement bar	2-noded truss element (embedded)

[22]. The parameter w_d in Table 3 is the limiting displacement at which concrete entirely loses its compressive strength. After concrete cracks, the compressive strength in the direction parallel to the cracks is reduced similarly to the MCFT [23]. The compressive strength reduction parallel to the crack direction is limited to, $r_c^{lim}f_c^{'}$. In this paper, based on parametric studies by Setiawan et al. [9], w_d was taken as 0.5 mm and $r_c^{lim}f_c^{'}$ as 0.8 $f_c^{'}$. Table 3 summarises the material parameters and modelling procedure adopted in ATENA. Reinforcement is modelled with a bilinear stress–strain relationship assuming perfect bond. Force-control in conjunction with the arc-length method was used along with the displacement, residual force, absolute residual force and energy error convergence criteria listed in Table 3. As in [9,24], a gradated mesh was used for the slab with the finer mesh used around the column up to a distance of twice the slab effective depth (d) away from the column face in each direction. Linear order hexahedra elements were used for concrete and linear order tetrahedra elements for steel loading plates.

If the load-rotation response of ATENA [8] did not show a clear peak and subsequent softening, the strain-based failure criterion of [6] was adopted. In this approach, punching shear failure is assumed to occur when the radial strain in the slab soffit measured at a distance of 0.5d away from the column face first reduces to zero. This approach is derived from the experimental observations of Ferreira et al. [25] and is similar to the punching failure criterion in the analytical model of Broms [26].

2.2. Corner joint shell punching model

This paper extends the JSPME [18,24] to include corner columns. The JSPM is implemented in the software ADAPTIC [27,28] and has previously been shown to give excellent predictions of punching resistance for internal columns [9] and edge columns [18,24]. In the JSPME, nonlinear joint elements are used to model punching shear failure. The joints are placed around the MC2010 punching control perimeter and connect the shell elements to either side of the control perimeter. Prior to punching shear failure, the joint out-of-plane shear stiffness is assumed to be rigid. Subsequently, the joint shear force is equated to the punching shear resistance which is calculated for each joint using the mean strength CSCT failure criterion of Muttoni [2] as follows:

$$V_{ji} = l_{si}\frac{3/4\sqrt{f_c^{'}}d}{1+15\frac{\psi_{si}\cdot d}{16+d_g}} \tag{13}$$

in which l_{si} is the joint spacing, $f_c^{'}$ (MPa) is the concrete cylinder strength, d_g (mm) is the maximum aggregate size, d (mm) is the slab average effective depth and ψ_{si} (radians) is the relative slab-column sector rotation for joint i which is extracted along the line of radial contraflexure. More details are given in [9,18,24].

A rigid plastic response is used to describe the torsional response of each joint. The joint torsional resistance, depicted T_{cri}, is determined [18,24] using the approach of Hsu [29] as implemented by Liu et al. [30,31]:

$$T_{cri} = 0.217 l_{si}\left(h^2+6450\right).\sqrt[3]{f_c^{'}} \quad (Nmm) \tag{14}$$

in which l_{si} and h (in mm) are the joint spacing and slab thickness respectively and f_c' (MPa) is the concrete compressive strength.

In the JSPME, the slab is modelled with 2-D nonlinear shell elements [32] incorporating the Reissner-Mindlin hypothesis. The punching shear joints are modelled with *jel 3* [27,28] elements. Each *jel 3* element is defined using 4 nodes as shown in Fig. 8 for a typical corner slab-column connection. Nodes 1 and 2, which are initially coincident, are located on the critical punching shear perimeter. Node 3 is located in the same sector as nodes 1 and 2 at the point of maximum slab-column rotation (near the line of radial contraflexure). Node 4 is located on the column chord (immediately above the slab) and is used to define the plane in which the y-axis is placed [6]. The relative radial slab-column rotation ψ_{si} in equation (13) is found from the difference between the rotations at nodes 3 and 4. The rotations are calculated individually for each joint and are updated at each loading step. In cases where the corner column side length exceeds 3d, the punching shear joints are positioned around a reduced control perimeter (see Fig. 1b). Dummy joints with minimal shear resistance are positioned along the neglected parts of the control perimeter. Similarly to edge columns [24], punching failure is assumed to result from failure of the most critically loaded of the punching shear joints positioned at i) the least of 0.5c_1 and 1.5d from the inner column face along c_1 and ii) the least of 0.5c_2 and 1.5d from the inner column face along c_2.

3. Validation of NLFEA modelling procedures against test results

This section demonstrates the ability of ATENA and the JSPME to capture the failure load of corner column punching test specimens from the literature. Results are presented for selected slabs tested by Walker and Regan [15], Zaghlool [16] and Hammill and Ghali [10].

Walker and Regan [15] tested 12 single panel slabs supported on corner columns. The first seven slabs (SC1 to SC7) were 3.05 m square and 125 mm thick. The corner columns measured either 300 mm square or 220 mm square and extended 1.25 m above and below the slab. The column ends were restrained laterally by pin-ended members located at a distance of 1.24 m above and below the central plane of the slab.

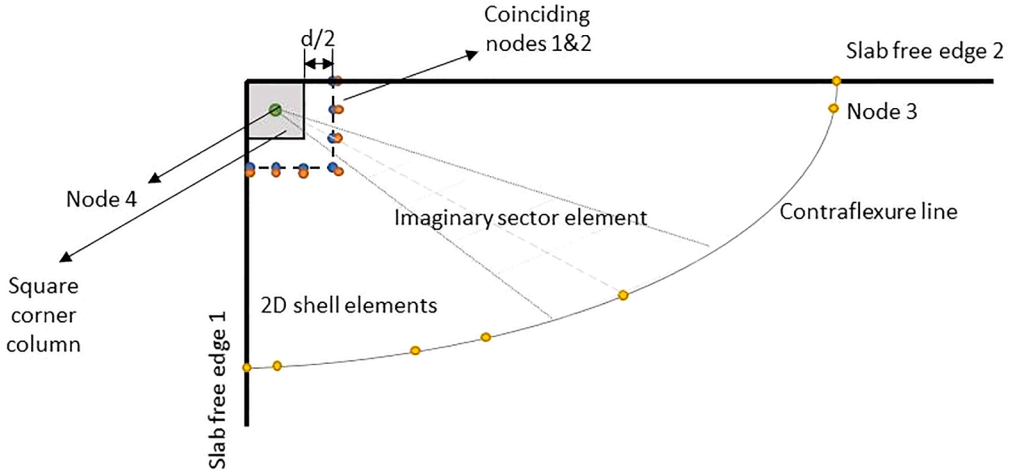

Fig. 8. JSPME for corner column-slab connections.

Uniform slab loading was simulated with 12 equal point loads. The remaining 5 slabs were 80 mm thick and either square (SC8-SC10) with side length of 2 m or rectangular (SC11-SC12) with side lengths 2 m × 1.4 m. The corner columns in slabs SC8-SC12 only extended below the slabs. In these specimens, uniform slab loading was simulated with either 12 (SC11-SC12) or 16 (SC8-SC10) point loads. Further details of these tests are given in [15] and Table 1. Fig. 9a and 9b which are representative show the finite element meshes adopted in ATENA and the JSPME respectively for slab SC8.

Fig. 10 compares the experimental load deflection responses of slabs SC1 to SC3, SC8 and SC9 with the responses obtained with ATENA and the JSPME. The ADAPTIC load–deflection response with 2-D shell elements but no *jel 3* elements is also included in Fig. 10a and 10b for comparison with the JSPME response. The introduction of joint elements in the JSPME is seen to have no influence on the load deflection response of these slabs. Overall, the JSPME load deflection response compares most favourably with the experimentally observed response, but ATENA gives the best estimate of failure load. Fig. 10a and 10b show that the ATENA load displacement responses for SC8 and SC9 have respectively a softening branch and well defined horizontal plateau at peak load. Fig. 10a and 10b also show that the strain-based failure criterion of [6] gives virtually the same peak load as ATENA, thereby justifying use of the criterion. The strain criterion, which has previously been validated for internal [6] and edge columns [18,24] assumes punching failure to occur when the radial compressive strain measured at 0.5*d* away from

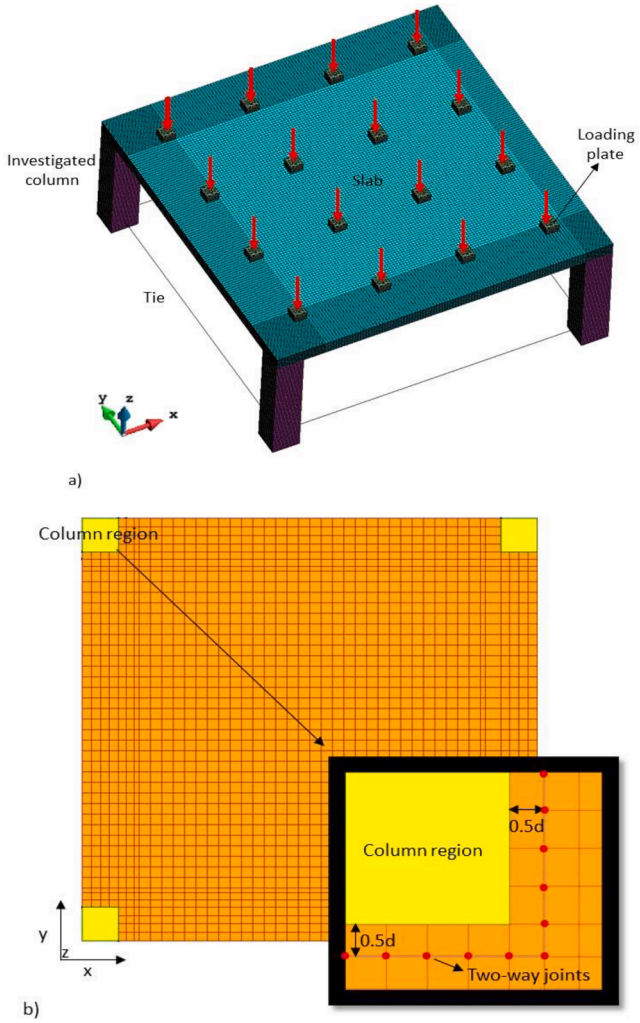

Fig. 9. Mesh configuration and boundary conditions for slab SC8 of Walker and Regan [15] in a) ATENA and b) the JSPME in ADAPTIC.

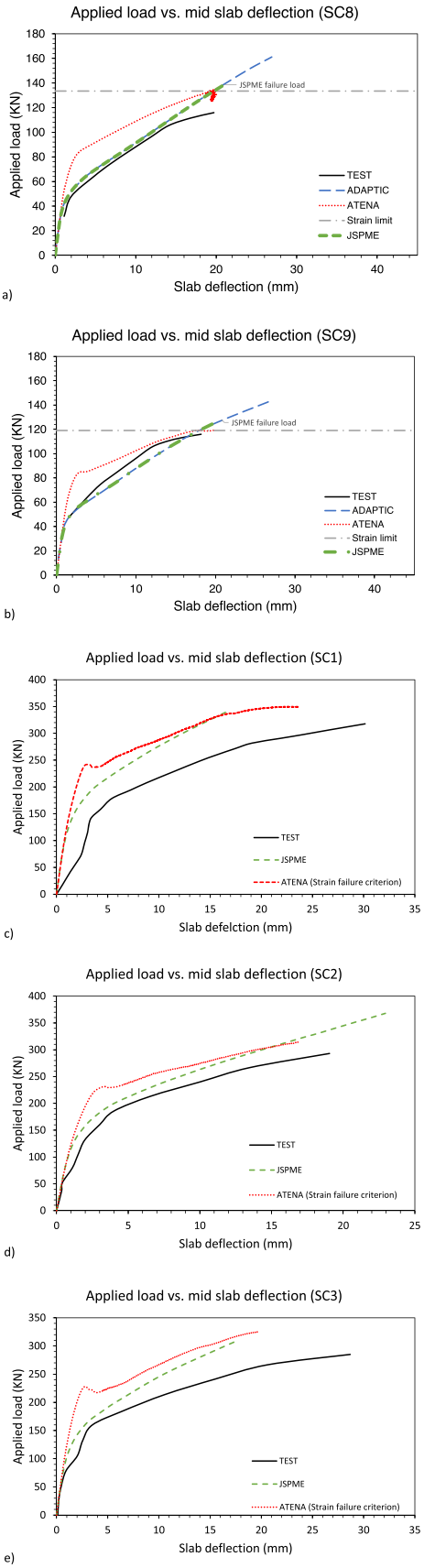

Fig. 10. Comparison of measured and predicted load vs mid slab deflection response for slabs a) SC8, b) SC9, c) SC1, d) SC2 and e) SC3 of Walker and Regan [15].

the column face in the slab soffit first drops to zero. This approach is needed for specimens like SC2 and SC3 where no distinct softening branch or horizontal plateau develops in the load displacement response at punching failure.

Table 4 compares measured and calculated punching shear resistances for selected slabs from Table 1. The calculated punching resistances were obtained with ATENA, the JSPME and the classic CSCT using the mean failure criterion of Muttoni [2]. The shear resisting perimeter in the classic CSCT was derived using k_e (see Equation (2) from MC2010. CSCT predictions are given for both the measured eccentricity at punching failure and the elastic eccentricity which is typically used in design. Table 4 also gives the measured, JSPME and elastic loading eccentricities, relative to the column centreline, along the slab edges at failure. The eccentricities were equal along each slab edge.

Table 4 shows that the ATENA strength predictions are consistently good, whilst the CSCT predictions are more variable partly due to their sensitivity to the adopted load rotation curve which is software dependent. The relative slab column rotation is not reported for the test specimens, so it is not possible to determine whether the variability of accuracy of the CSCT predictions is due to inaccuracies in estimating the rotation or the failure criterion itself. The relatively large difference between the JSPME and MC2010 failure loads in Table 4 for the isolated specimens is due to different rotations being used for each. If the ADAPTIC rotations, which are overly stiff at low eccentricities, are used instead of ATENA rotations, the MC2010 predictions for Z1(1), ZII (1) and ZII (6) become 0.77, 0.91 and 0.94 compared with 0.76, 0.83 and 1.00 from the JSPME.

3.1. Modelling of virtual corner slab-column connections with non-square columns

NLFEA was used to simulate punching failure at non-square corner columns which have not been tested experimentally. The results of the analyses are used to further validate the punching provisions in FprEN1992. The geometry of the slab considered in the parametric studies is derived from specimens NH1, NH2 and NH4 of Hammill and Ghali [10]. These slabs measured 1075mm long, 1075mm wide and 150 mm thick as shown in Fig. 11 with an average effective depth of 114mm. The corner column measured 250x250mm^2. Slab edges opposite to the column were simply supported. Combined vertical and horizontal loads were applied through the column. The study investigated the effect of varying the loading eccentricity and column size. This was achieved by extending the slab and column backwards by a distance x to form the longer column dimension and sideways by 50 mm (see Fig. 11) to form column sizes of 600 x 300, 750 x 300 and 1000 x 300 mm^2. The tensile reinforcement ratio was slightly increased from that in specimen NH4 to prevent flexural failure. The variables of the parametric studies are listed in Table 5 below. A practical range of eccentricities was determined for each column size based on the analysis of a series of full-scale floor plates in ETABS [19]. Equal eccentricities (depicted $e_{col,x}$ and $e_{col,y}$) relative to the column centreline were adopted along each slab edge which is onerous for the rectangular columns at large eccentricities. The concrete compressive strength was taken as 36.9 MPa as in specimen NH4.

The shear resistance of the specimens summarised in Table 5 was determined using:

- ATENA [8]
- JSPME
- Classic CSCT (MC2010 LoA IV with mean CSCT failure criterion of [2]) with k_e calculated using MC2010 (see equation (2)) [3].
- FprEN1992 with β from equations (11) and (12) (refined) and $\beta = 1.5$ with M_{tmax} limit.
- EC2 [5] with M_{tmax} limit

Results of the simulations are given in Table 6 and Fig. 12 which show the effect of loading eccentricity on the predicted shear resistance for each method. Comparison with Fig. 5a suggests that the results for $1.1(|e_x|+|e_y|)/b_b$ greater than 2.5 are extreme cases which are unlikely to arise in practice. Based on the analysis of test specimens in Table 5, the ATENA strength predictions in Table 5 are considered to be most accurate. All three of the code predictions in Table 5 are close to the ATENA predictions for these specimens but this is largely due to M_{tmax} governing at larger eccentricities for EC2 (2004) and FprEN 1992 with $\beta = 1.5$. Without the limitation of M_{tmax}, all the EC2 (2004) predictions become unsafe relative to ATENA at the maximum considered eccentricity. This is concerning since the M_{tmax} limit only appears in Annex I of EC2 (2004) which is informative. The M_{tmax} limit is unnecessary when using the refined β (see equations (11) and (12) in FprEN 1992 but necessary for $\beta = 1.5$. However, the authors consider application of the M_{tmax} limit to be good practice in all cases. The MC2010 LoA IV failure loads are given by the intersection of the CSCT resistance curve and the load-rotation curve, which was determined using both ATENA [8] and ADAPTIC [27,28]. Table 6 shows that the resulting strength predictions with ATENA rotations tend to be slightly less than obtained with ADAPTIC rotations. The JSPME strength predictions are on average closest to those obtained with CSCT LoA IV using ATENA rotations. The classic CSCT and JSPME punching resistances are significantly less than the other predictions, including EC2 (2004), for the 300 × 1000 mm^2 column. The FprEN 1992 results are considered acceptable in this case given their closeness to the predictions of ATENA and EC2 (2004) but experimental confirmation is recommended.

The reason for the differences between the LoA IV resistances obtained with rotations from ATENA and ADAPTIC is illustrated in Fig. 13a. The figure compares load rotation responses obtained with

Table 4
Comparison of measured and NLFEA strengths of selected slabs from Table 1.

Slab notation	e_{test} (mm)	$e_{elastic}$ (mm)	e_{JSPME} (mm)	V_{Test} (KN)	V_{Test}/V_{ATENA}	V_{Test}/V_{JSPME}	V_{Test}/V_{MC2010}	
							$e_{elastic}$	e_{test}
Z1 (1) [16]**	258	258	258	74.3	1.004	0.762	0.929	0.929
ZII (1) [16]**	279	279	279	137.9	1.379	0.831	1.365	1.365
ZII (6) [16]**	473	473	473	82.3	1.004	1.001	1.016	1.016
SC1 [15]*	309	378	372	81.5	0.933	0.891	0.776	0.731
SC2 [15]*	321	378	327	74.8	0.950	0.796	0.733	0.700
SC3 [15]*	426	378	389	74.2	0.913	0.907	0.765	0.789
SC8 [15]*	142	223	158	33.0	0.979	0.951	0.917	0.786
SC9 [15]*	179	223	180	33.0	0.885	1.031	0.971	0.887
NH1 [10]**	293	293	293	146.9	1.023	0.816	1.224	1.224
NH2 [10]**	289	289	289	139.1	1.008	0.740	1.149	1.149
				Mean	**1.008**	**0.873**	**0.985**	**0.958**
				Standard deviation	**0.138**	**0.100**	**0.209**	**0.226**

** The load-rotation response from ATENA was used to obtain V_{MC2010}. * The load-rotation response from ADAPTIC was used to obtain V_{MC2010}.

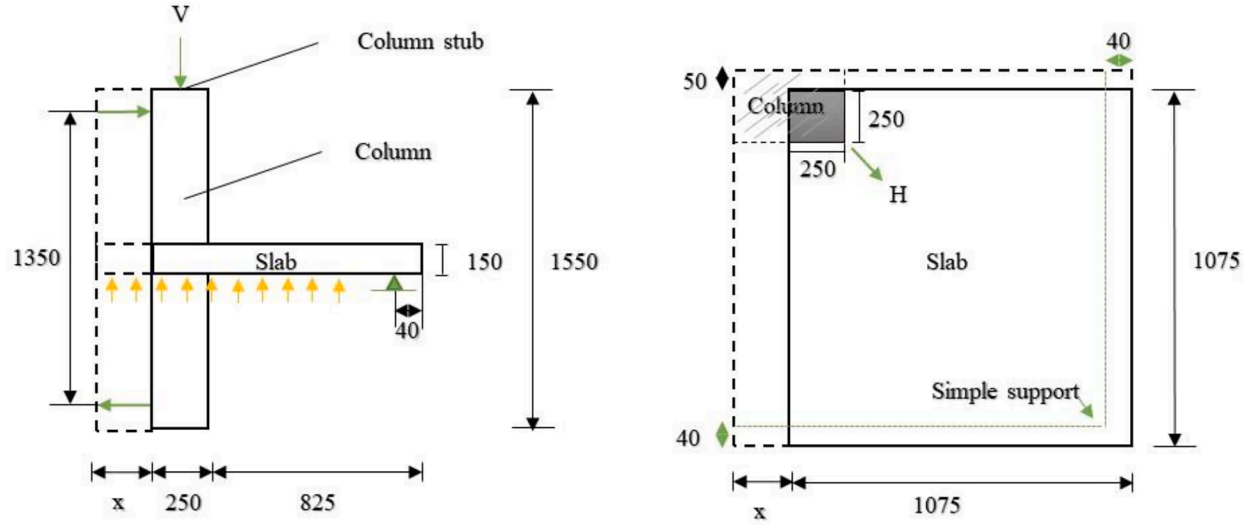

Fig. 11. Elevation (left) and plan (right) of slab NH4 [10] and extended virtual slab (All dimensions in mm).

Table 5
Details of investigated virtual corner slab-column connections.

Slab notation	Column dimensions (mmxmm)	Loading eccentricities ($e_{col,x}$) and ($e_{col,y}$) along each slab edge (mm)	%ρ around the column region
NH4 250 × 250	250 × 250	300, 400 & 500	2.00
NH4 300 × 600	300 × 600	600, 700 & 800	2.00
NH4 300 × 750	300 × 750	600, 700 & 1000	2.10
NH4 300 × 1000	300 × 1000	800, 900 & 1100	2.20

each software for specimen NH4 with column size 300 x 600 mm^2 and eccentricities, relative to the column centreline, of 600 mm and 800 mm. Also shown in Fig. 13a are the CSCT resistance curves for each loading eccentricity. In these, the influence of loading eccentricity on the resistance is accounted for through the multiplier k_e from Equation (2). The CSCT failure load is given by the intersection of the load-rotation and load-resistance curves. Initially, the ATENA and ADAPTIC load-rotation responses are similar but towards failure the ATENA response is softer resulting in a lower failure load.

As shown in Fig. 13a, the rotation increases with loading eccentricity. Consequently, even for fixed k_e (see equation (1) the predicted failure load reduces with loading eccentricity. The effect of reducing k_e is to reduce the failure load. However, as evident in Fig. 13a the reduction in failure load is less than proportional to k_e. This is the case since the reduction in failure load due to reducing k_e is accompanied by a reduction in rotation which is associated with an increase in resistance. This lack of proportionality between k_e and punching resistance in the classic CSCT explains why β in the closed form CSCT does not equal $1/k_e$.

An advantage of the JSPME over the classic CSCT is that the JSPME models shear redistribution around the control perimeter of the type identified by Sagaseta et al. [33]. Furthermore, the JSPME circumvents the need to make use of k_e in the calculation of the shear resisting perimeter as done in MC2010 LoA IV. The influence of shear redistribution is illustrated in Fig. 13b for slab NH4 (300 x 600 mm^2) with $e_{col,x} = e_{col,y} = 600$mm. For this specimen the failure loads given by ATENA and the JSPME are very similar. The figure shows the shear force distributions around the control perimeter from i) ATENA at V_{ATENA}, ii) the JSPME at V_{JSPME} and iii) elastic analysis with ADAPTIC at V_{ATENA}. All three curves are similar but the peak shear forces are less in the nonlinear analyses due to shear redistribution. Shear redistribution occurs in the JSPME due to nonlinear shell element behaviour as well as redistribution of shear forces from failing to non-failing joint elements. Consideration of Fig. 13b shows that it is over conservative to assume

Table 6
Punching shear predictions for virtual corner slab-column connections.

Slab	$e_{col,x} = e_{col,y}$ (mm)	V_{ATENA}/V_{JSPME}	V_{ATENA}/V_{MC2010}		$V_{ATENA}/V_{FprEN1992}$		$V_{ATENA}/V_{EC2\ (2004)}$
			ADAPTIC rotation	ATENA rotation	β refined	β = 1.5	
NH4 250x250	300	0.97	1.27	1.23	1.29	1.40	1.39
	400	1.15	1.16	1.17	1.16	1.11	1.10
	500	1.32	1.01	1.11	1.02	1.00	0.98
NH4 300x600	600	1.04	0.96	1.03	1.09	1.05	1.03
	700	1.26	1.16	1.17	1.18	1.17	1.14
	800	1.31	1.25	1.23	1.11	1.17	1.14
NH4 300x750	600	1.03	0.99	1.11	1.16	1.16	1.15
	700	1.14	0.94	1.04	1.06	0.99	0.98
	1000	1.14	1.11	1.23	0.83	0.91	0.90
NH4 300x1000	800	1.37	1.25	1.44	1.20	1.12	1.11
	900	1.32	1.29	1.46	1.10	1.05	1.03
	1100	1.34	1.33	1.47	0.95	1.00	0.98
Mean		**1.20**	**1.14**	**1.22**	**1.10**	**1.09**	**1.08**
Standard deviation		**0.14**	**0.14**	**0.16**	**0.12**	**0.13**	**0.13**

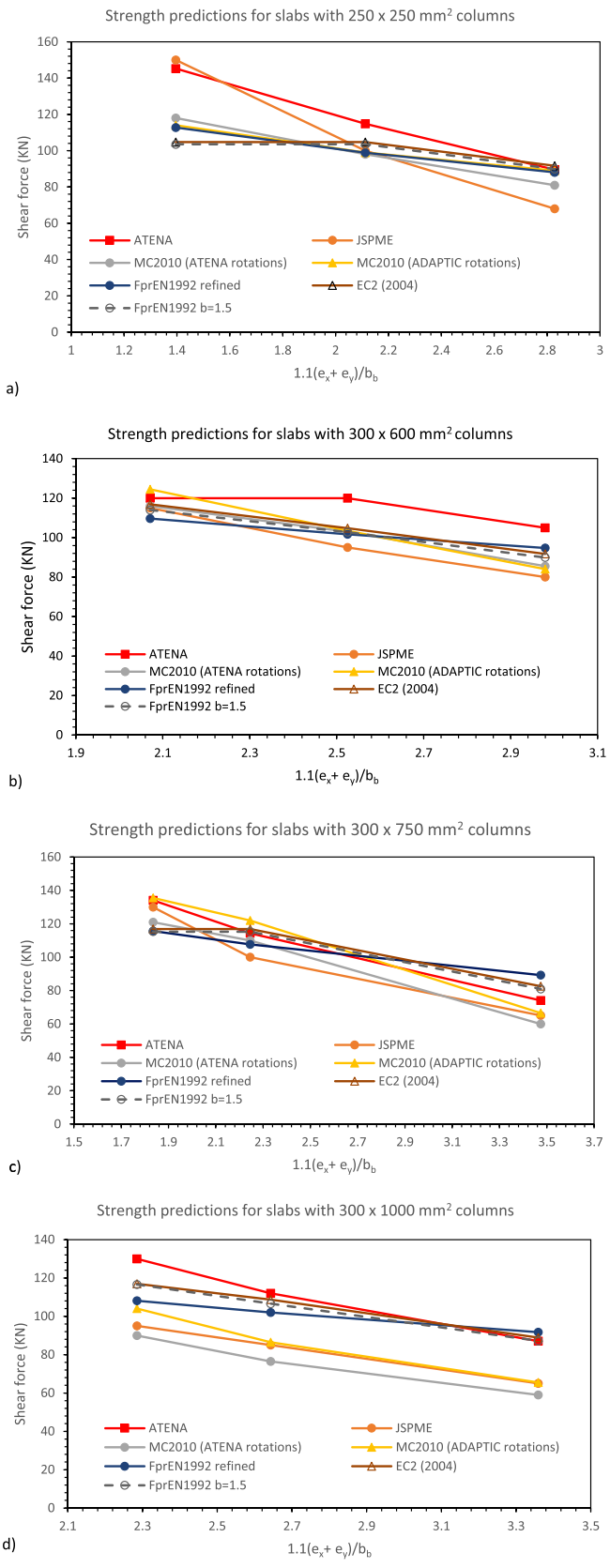

Fig. 12. Punching shear resistance for virtual corner column punching specimens with column size a) 250 x 250 mm^2, b) 300 x 600 mm^2, c) 300 x 750 mm^2 and d) 300 x 1000 mm^2.

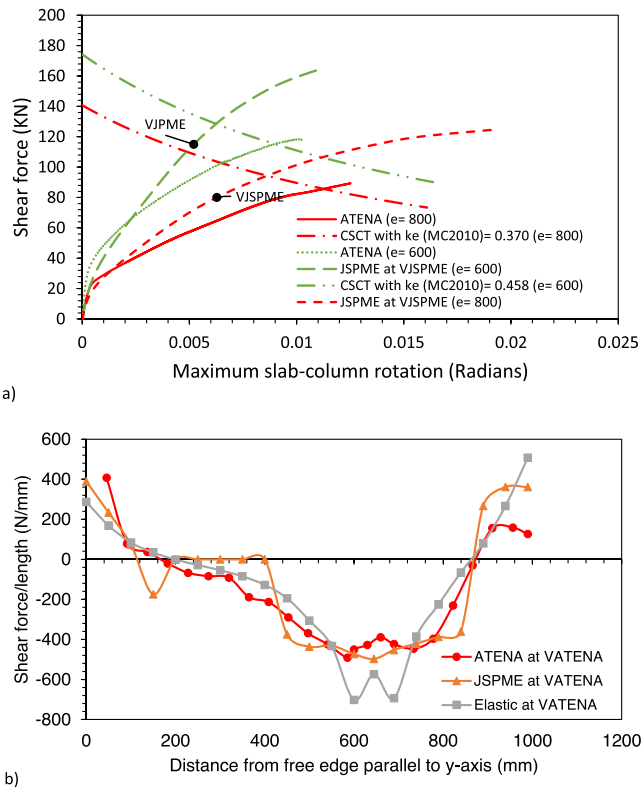

Fig. 13. Response of virtual specimen NH4 with column size 300 x 600 mm^2 a) ATENA and JSPME load-rotation responses for eccentricities $e_{col,x} = e_{col,y}$ of i) 600mm and ii) 800mm and b) shear force/length distribution around the control perimeter for $e_{col,x} = e_{col,y} = 600$ mm.

that punching failure occurs when the peak elastic shear force per unit length around the control perimeter equals the design shear resistance as assumed in MC2010. Instead, some averaging of shear force to either side of the peak value is permissible as proposed by Sagaseta et al [33] and allowed in FprEN1992.

As a reality check, design punching resistances, without shear reinforcement, were calculated for the full scale flat slab specimens considered in the derivation of β_{SF} (see Fig. 5) with i) EC2 (2004) and ii) FprEN1992 using the refined β (see equations (11) and (12)). The EC2 (2004) resistances were calculated with the reduced control perimeter u_{1*} of the code and the M_{tmax} limit. In FrEN1992, a_{pd} was conservatively taken as d_v in equation (5). The code recommended partial factors of $\gamma_c = 1.5$ and $\gamma_v = 1.4$ were adopted in EC2 (2004) and FprEN1992 respectively. $V_{FprEN1992}/V_{EC2}$ is plotted against the normalised loading eccentricity in Fig. 14a which shows that both codes give similar punching resistances. Furthermore, Fig. 14b shows that $V_{FprEN1992}/V_{EC2}$ is sensibly independent of the loading angle.

4. Conclusions

This paper describes the derivation of the shear enhancement factor β for punching shear at corner columns in the next generation of EC2 (FprEN 1992) which adopts a closed form formulation of the CSCT for punching shear. In this method, the effect of loading eccentricity on punching resistance is accounted for by increasing the design shear force by a multiple β. Initially, a formula is derived for β using shear field analysis of representative flat slab buildings. The adopted procedure is the same as that previously adopted by the authors for determination of β at edge columns in FprEN1992. The resulting formulae for β have the same form at edge and corner columns (i.e. $\beta = 1 + 1.1\frac{e_b}{b_b}$) but the eccentricity e_b is defined differently in each case owing to differences in the shear force distribution around the control perimeter at edge and

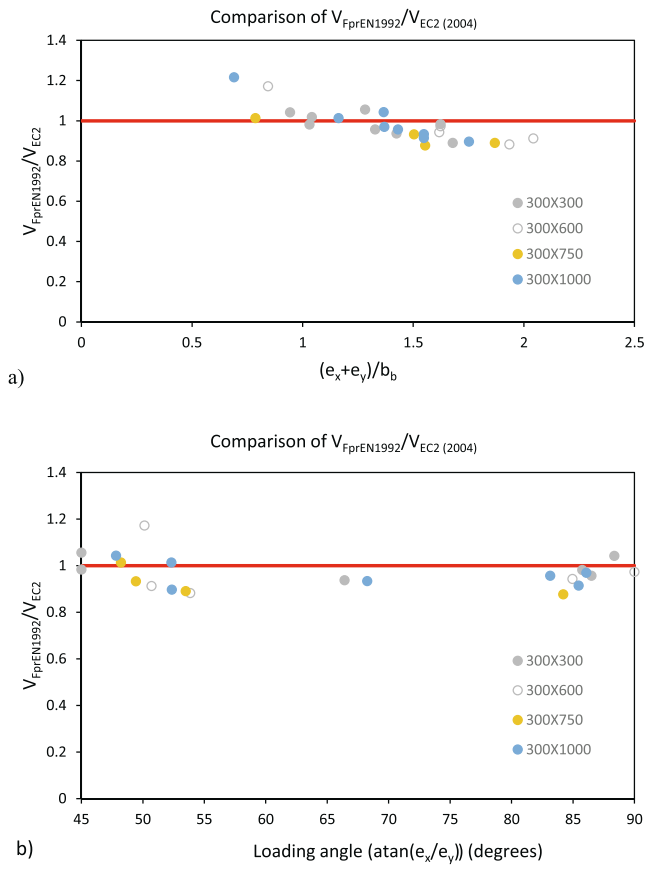

Fig. 14. Influence on $V_{FprEN1992}/V_{EC2\ (2004)}$ of a) loading eccentricity and b) loading angle on punching resistance of specimens in Fig. 5.

corner columns.

The expression for β resulting from shear field analysis is validated using experimental data from the literature as well as virtual specimens, with elongated columns, modelled with NLFEA using both 3-D solid elements and the classic CSCT. Even though used to derive the refined expression for β, shear field analysis is not recommended for routine design due to the sensitivity of the results to modelling assumptions and software used. Finally, FprEN1992 is shown to give similar punching resistances to EC2 (2004) at corner columns of representative flat slabs without shear reinforcement. Significantly, the refined formula for β (see equations (11) and (12)) gives significantly lower values than the reciprocal of the expression for k_e used in MC2010 to reduce the control perimeter for eccentric shear.

When used in conjunction with the refined expression for β, FprEN1992 is shown to give good estimates of punching resistance at corner columns for both the considered test data and the virtual slabs modelled with 3-D solid elements in ATENA. Due to the relative lack of experimental data on punching at corner columns, the authors recommend conservatively taking $a_{pd} = d_v$ in equation (6) if using the refined β.

Declaration of Competing Interest

The authors declare that they have no known competing financial interests or personal relationships that could have appeared to influence the work reported in this paper.

References

[1] CEN/TC 250/SC 2 FprEN 1992-1-1:2022: Eurocode 2: Design of Concrete Structures - Part 1-1: General rules for buildings, bridges and civil engineering structures. 2022.
[2] Muttoni A. Punching shear strength of reinforced concrete slabs without transverse reinforcement. ACI Struct J 2008;105(4):440–50.
[3] fib (Fédération International du Béton). fib Model Code for concrete structures. Lausanne, Switzerland: Fédération International du Béton; 2010. p. 2013.
[4] Muttoni A, Ruiz MF, Simoes JT. The theoretical principles of the critical shear crack theory for punching shear failures and derivation of consistent closed-form design expressions. Struct Concr 2018;19(1):174–90.
[5] BSI. BS EN 1992-1-1:2004. Eurocode 2, design of concrete structures – part 1–1: general rules and rules for buildings. London, UK: BSI; 2004.
[6] Setiawan A, Vollum RL, Macorini L, Izzuddin B. Punching of RC slabs without transverse reinforcement supported on elongated columns. Structures 2020;27:2048–68.
[7] Setiawan A, Vollum RL, Macorini L, Izzuddin BA, 2020, Punching shear design of RC flat slabs supported on wall corners, *Struct Concr*, 21, 859–874, ISSN: 1464-4177.
[8] Cervenka V, Jendele L, Cervenka J. ATENA Program Documentation, Part 1, Theory. Cervenka Consulting: Prague; 2018. p. 334.
[9] Setiawan A, Vollum RL, Macorini L, Izzuddin B. Efficient 3-D modelling of punching shear failure at slab-column connections by means of nonlinear joint elements. Eng Struct 2019;197:109372.
[10] Hammill N, Ghali A. Punching shear resistance of corner slab-column connections. ACI Struct J 1994;91(6):697–705.
[11] Ingvarsson, H., Experimentellt stadium av betongplattor understödda av hörnpelare, (Experimental study of concrete slabs supported by corner columns), Meddelande Nr. 111, Institutionen för byggnadsstatik, kungliga tekniska högskolon, Stockholm, 1974, 26 pp.
[12] Stamenkovic A, Chapman J. Local strength at column heads in flat slabs subjected to a combined vertical and horizontal loading. Instit Civil Eng 1974;57(2):205–32.
[13] Sudarsana IK. Punching shear in edge and corner column slab connections of flat plate structures. University of Ottawa; 2001. PhD thesis.
[14] Vocke H. Zum Durchstanzen von flachdecken im Bereich von Rand-und Eckstützen. *Dissertation*. Institut für Werkstoffe im Bauwesen, Universität Stuttgart; 2002. p. 284.
[15] Walker P, Regan P. Corner column-slab connections in concrete flat plates. J Struct Eng 1987;113(4):704–20.
[16] Zaghlool E. Strength and behaviour of corner and edge column-slab connections in reinforced cocnrete flat plates. The University of Calgary; 1971. PhD Thesis.
[17] Zaghlool R, Rawdon de Paiva H, Glockner P. Tests of reinforced concrete flat plate floors. J Struct Div Proc Am Soc Civ Eng 1970;96(3):487–507.
[18] Abu-Salma D, Vollum RL, Macorini L. Design of biaxially loaded external slab column connections. Eng Struct 2021;249:1–16.
[19] Computers and Structures, Inc. ETABS V-2017 (Student version). Integrated finite element analysis and design of structures.
[20] Goodchild CH, Webster RM, Elliott KS. Economic concrete frame elements to eurocode 2. Surrey The Concrete Centre; 2009.
[21] Menetrey P, Willam KJ. Triaxial failure criterion for concrete and its generalization. ACI Struct J 1995;92(3):311–8.
[22] van Mier JGM. Multi-axial strain-softening of concrete, Part I: fracture, Part II: load histories. Mater Struct, RILEM 1986;19(3):179–90.
[23] Vecchio FJ, Collins MP. The modified compression-field theory for reinforced concrete elements subjected to shear. ACI Struct J 1986;83(2):219–31. https://doi.org/10.1016/j. engstruct.2019.109372.
[24] Abu-Salma D, Vollum RL, Macorini L. Modelling punching shear failure at edge slab-column connections by means of nonlinear joint elements. Structures 2021;2021(34):630–52.
[25] Ferreira MP, Melo GS, Regan PE, Vollum RL. Punching of reinforced concrete flat slabs with double-headed shear reinforcement. ACI Struct J 2014;111(2):363–74.
[26] Broms CE. Tangential strain theory for punching failure of flat slabs. ACI Struct J 2016;113:95–104.
[27] Izzuddin, BA. Nonlinear dynamic analysis of framed structures. PhD Thesis. Imperial College London; 1991.
[28] Izzuddin, B.A., 2016, ADAPTIC User Manual, Imperial College London, https://www.imperial.ac.uk/media/imperial-college/research-centres-and-groups/computational-structural-mechanics/ADAPTIC_Manual.pdf.
[29] Hsu TTC. Torsion of structural concrete-behavior of reinforced concrete rectangular members. ACI Special Publication 1968;18–08:261–306.
[30] Liu J, Tian Y, Orton SL, Said AM. Resistance of flat-plate buildings against progressive collapse. Part I: Modelling of slab-column connections. J Struct Eng 2015;141(12).
[31] Liu J, Tian Y, Orton SL, Said AM. Resistance of flat-plate buildings against progressive collapse. Part II: system response. J Struct Eng 2015;141(12).
[32] Izzuddin BA, Tao XY, Elghazouli AY. Realistic modeling of composite and reinforced concrete floor slabs under extreme loading. Part I: Analytical Method. J Struct Eng 2004;130(12):1972–84.
[33] Sagaseta J, Muttoni A, Fernandez Ruiz M, Tassinari L. Non-axis-symmetrical punching shear around internal columns of RC slabs without transverse reinforcement. Mag Concr Res 2011;63(6):441–57.